Electro Production of π^0 near the Threshold

Author: Miha Mihovilovič (28030004)
Mentor: doc. dr. Simon Širca

January 19, 2009

Abstract

In this seminar I will make a quick introduction into the Chiral Perturbation theory (ChPT) and try to explain its basic ideas. I will apply the general principles of ChPT to neutral pion electroproduction on the proton near threshold, show the stucture of the corresponding Lagrangian. Then I will compare the predictions of the theory to existing measurements and point out the most evident differences between them. In the end I will focus on a particular experiment (E04-007) at Jefferson Lab, which was designed to extend and re-examine existing measurements, in particular those from Mainz.

Contents

1 Overture into Quantum Chromodynamics

Strong interaction is a fundamental force between quarks and gluons inside the hadrons. A theory that describes this interaction is Quantum chromodynamics (QCD) [1, 2, 3] and is an important

part of the Standard Model of particle physics [4].

QCD introduces six fundamental particles (quarks) and eight interaction particles, called gluons. Their dynamics is controlled by the Lagrangian:

$$L_{QCD} = \overline{q_i}\left(i\gamma^\mu\partial_\mu - m\right)q_i - \frac{1}{4}G^a_{\mu\nu}G^{\mu\nu}_a - gG^a_\mu\overline{q_i}\gamma^\mu\lambda^a_{ij}q_j, \quad a = 0\ldots 8 \tag{1}$$

where q_i and G^a_μ are quark and gluon fields, and λ^a are the generators of the SU(3) group. The first term in the Lagrangian corresponds to free-quark dynamics, the second part represents the dynamics of the gluons, while the third part describes the interaction between quarks and gluons. Regarding the Strong interaction, quarks of different flavors (u,d,s,c,b,t) have identical properties except for their masses. Quark masses are free parameters in QCD which means that the theory can be formulated for any value of quark masses. If we restrict the theory only to the light quarks, QCD can be well approximated with the fictitious massless quarks only. In this case the Lagrangian (1) would be symmetric to the exchange of quarks of different flavors. We call this a Flavor symmetry. In reality, the flavour symmetry is only approximate because the quarks have different masses.

In the massless limit we can also realize that the left- and right-handed quarks are completley decoupled:

$$\begin{aligned} L^{(m_i=0)}_{QCD} &= \overline{q}^L_i\left(i\gamma^\mu\partial_\mu\right)q^L_i - gG^a_\mu\overline{q}^L_i\gamma^\mu T^a_{ij}q^L_j + \\ &\quad + \overline{q}^R_i\left(i\gamma^\mu\partial_\mu\right)q^R_i - gG^a_\mu\overline{q}^R_i\gamma^\mu T^a_{ij}q^R_j - \frac{1}{4}G^a_{\mu\nu}G^{\mu\nu}_a, \end{aligned} \tag{2}$$

with $q_L = P_L q$ and $q_R = P_R q$, where P_L and P_R are projection operators [5], and are defined as:

$$P_L = \frac{1}{2}\left(1+\gamma_5\right), \quad P_R = \frac{1}{2}\left(1-\gamma_5\right).$$

The massless Lagrangian is therefore invariant under separate unitary global transformations of the left- and right-hand quark fields, known as the chiral rotations:

$$\begin{aligned} q'_L &= e^{i\epsilon_i T_i(1-\gamma_5)}q_L, \\ q'_R &= e^{i\delta_i T_i(1+\gamma_5)}q_R, \\ L'^{(m=0)}_{QCD}(q'_L, q'_R) &= L^{(m=0)}_{QCD}(q_L, q_R) \end{aligned}$$

where ϵ_i and δ_i are free parameters of the transformations and T_i are the Gell-Mann matrices $T_i = \frac{1}{2}\lambda_i$. This property of QCD is called Chiral symmetry. The chiral symmetry transformations L, R can be rewritten into a symmetric vector and antisymmetric axial-vector symmetry transformations:

$$\begin{aligned} V &\sim \left(e^{i\epsilon_i T_i(1-\gamma_5)} + e^{i\delta_i T_i(1+\gamma_5)}\right) = e^{i\phi_a T_a}, \\ A &\sim \left(e^{i\epsilon_i T_i(1-\gamma_5)} - e^{i\delta_i T_i(1+\gamma_5)}\right) = e^{i\theta_a T_a\gamma_5}, \end{aligned}$$

where θ_i and ϕ_i are again transformation parameters. Now we can introduce the Vector and Axial currents as [2]:

$$\begin{aligned} V^\mu_a &= \frac{\partial L}{\partial(\partial_\mu\phi_a)} = \overline{q}\gamma^\mu\frac{\lambda_a}{2}q, \\ A^\mu_a &= \frac{\partial L}{\partial(\partial_\mu\theta_a)} = \overline{q}\gamma^\mu\gamma_5\frac{\lambda_a}{2}q, \end{aligned}$$

where $a = 0, \ldots 8$ and $\lambda_0 = 1$. We get nine vector and nine axial currents. If chiral symmetry is a good symmetry for a given Lagrangian, than these currents are conserved by virtue of the Noether's theorem [2]:

$$\partial_\mu V_a^\mu = 0, \quad \partial_\mu A_a^\mu = 0\,.$$

In QCD these relations are true in the limit of massless quarks. However, we know that quark masses are not exactly zero. The nonzero quark mass leads to the so-called explicit chiral symmetry breaking and consequently, the Vector and Axial-vector currents are no longer conserved [3]:

$$\begin{aligned} \partial_\mu V_a^\mu &= \frac{1}{2} i\overline{q}\,[M, \lambda_a]\,q\,, \\ \partial_\mu A_a^\mu &= \frac{1}{2} i\overline{q}\,\{M, \lambda_a\}\,\gamma_5 q\,, \\ M &= \begin{pmatrix} m_u & 0 & 0 \\ 0 & m_d & 0 \\ 0 & 0 & m_s \end{pmatrix} \end{aligned} \tag{3}$$

However, the consequences of the explicit symmetry violation can still be analyzed systematically because quark masses are small. We say, that QCD possesses an approximate chiral symmetry. Let us also mention that QCD is also invariant under the discrete symmetries of parity (P), charge conjugation (C) and time reversal (T).

Beside symmetries QCD also has some other very interesting properties. Figure 1 shows that the Strong-coupling constant α_s, which is a measure for the strength of the interaction, decreases with increasing energy μ. This means that in high-energy reactions quarks and gluons interact very weakly. This prediction of the QCD was first discovered in the early 1970s by David

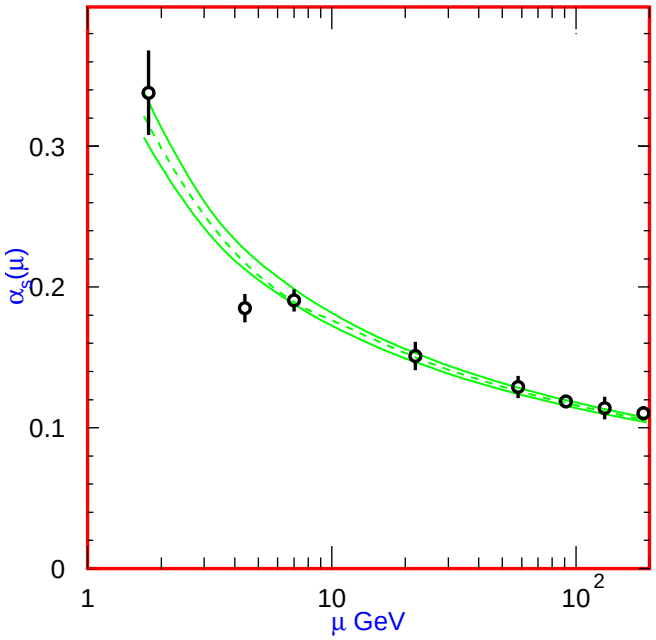

Figure 1: Summary of the values of $\alpha_s(\mu)$ at characteristic energies μ where they are measured. The lines show the central values and the $\pm 1\sigma$ limits of our average. The figure clearly shows the decrease in $\alpha_s(\mu)$ with increasing μ. The data are, in increasing order of μ, τ width, Υ decays, deep inelastic scattering, e^+e^- event shapes at 22 GeV from the JADE data, shapes at TRISTAN at 58 GeV, Z width, and e^+e^- event shapes at 135 and 189 GeV [4].

Politzer, Frank Wilczek and David Gross and is known as the Asymptotic freedom. For this discovery these authors were awarded the Nobel prize in 2004. It allows us to employ perturbative methods to analyze and understand the physical processes. On the other hand, at low energies

(or equivalently at large distances) the force between quarks becomes stronger and stronger. Because of that it would take an infinite amount of energy to separate two quarks and therefore they are forever bound into hadrons such as proton[1]. This property of the QCD is known as confinement. This low energy regime is beyond the reach of the perturbative theory and demands a non-perturbative treatment. The necessity to employ approaches for long-distance processes has encouraged scientists to develop various effective field theories. One such theory is Chiral Perturbation Theory.

2 The Chiral Perturbation Theory

Chiral perturbation theory [6] (ChPT) is an effective field theory constructed of an effective Lagrangian which is consistent with the chiral symmetry of quantum chromodynamics, as well as with other symmetries. In the ChPT we no longer use quarks and gluons as degrees of freedom. Instead we write an effective Lagrangian with hadrons (protons, pions) as our basic particles. The purpose of this effective Lagrangian method is to represent in a simple way the dynamical content of a theory in the low energy limit, where effects of heavy particles can be incorporated into a few constants [7]. The main idea in the ChPT is to write a Lagrangian which includes all terms consistent with the symmetries of the parent theory. In general there is an infinite number of such terms, but one hopes that at low energies only few will be relevant. The Lagrangian also contains unknown parameters, known as low-energy constants, which are associated with specific terms in the Lagrangian and must be determined by a numerical fit to various experimental data. The pion fields are usually represented in the exponential form [7]:

$$\overset{o}{U}= e^{\frac{i}{F}\phi}, \quad \phi = \begin{pmatrix} \pi^0 & \sqrt{2}\pi^+ \\ \sqrt{2}\pi^- & -\pi^0 \end{pmatrix}, \quad F = 132\,\mathrm{MeV}$$

The matrix U is used to generate the Lagrangian which is invariant under the chiral $SU(2)$ transformation:

$$\begin{aligned} L &= \sum_i L_i = L_2 + L_4 + L_6 + L_8 + \cdots = \\ &= \frac{F^2}{4} Tr\left(\partial_\mu \overset{o}{U}\, \partial^\mu \overset{o}{U}^\dagger\right) + \alpha_1 \left[Tr\left(\partial_\mu \overset{o}{U}\, \partial^\mu \overset{o}{U}^\dagger\right)\right]^2 \\ &\quad + \alpha_2 Tr\left(\partial_\mu \overset{o}{U}\, \partial_\nu \overset{o}{U}^\dagger\right) \cdot Tr\left(\partial^\mu \overset{o}{U}\, \partial^\nu \overset{o}{U}^\dagger\right) + \ldots . \end{aligned} \tag{4}$$

The terms without derivatives are not included in the Lagrangian, because $Tr\left(UU^\dagger\right) = 2$ is a constant. The indices i denote the order of a particular term in the Lagrangian. It follows from the dimensional analysis that the coefficient before an operator with n derivatives behaves as $\frac{1}{M^{n-4}}$, where M is a mass scale which depends on the specific theory [7]. We also know that each derivative gives us a factor of q when we calculate the matrix elements. That means, that the effect of an n-derivative vertex is of order:

$$L_n \propto \frac{q^n}{M^{n-4}} = M^4 \left(\frac{q}{M}\right)^n$$

Consequently we can write our Lagrangian symbolically as:

$$L = C_2 \left(\frac{q}{M}\right)^2 + C_4 \left(\frac{q}{M}\right)^4 + C_6 \left(\frac{q}{M}\right)^6 + \ldots \tag{5}$$

This kind of expansion is most commonly used and is known as momentum expansion.

[1] This is also the reason why we can not detect single quarks. We simply do not have enough energy to separate them from the hadrons.

2.1 Pion Electroproduction in the ChPT

In the following we apply the ChPT Lagrangian to the particular process of the electroproduction of a neutral pion on the proton. In the isospin limit ($m_p = m_n = m^0$) the Lagrangian to the first order looks like [3]:

$$
\begin{aligned}
L &= L_{\text{First Order}} + \cdots = L^{(1)}_{\pi N} + L^{(2)}_{\pi\pi} + \ldots && (6)\\
L^{(1)}_{\pi N} &= \overline{\psi}\left(i\gamma^\mu D_\mu - m_0\right)\psi + \frac{\alpha_s^0}{2}\overline{\psi}\gamma_\mu\gamma_5 u^\mu\psi && (7)\\
L^{(2)}_{\pi\pi} &= \frac{F^2}{4}Tr\left[\bigtriangledown_\mu U^\dagger \bigtriangledown^\mu U + M_0^2(U + U^\dagger)\right]
\end{aligned}
$$

The superscript in (6) denotes the energy dimension in terms of order q^i (see equation (5)) of each term. The tree level Lagrangian $L_{\text{First Order}}$ depends on the nucleon mass m^0, the strong coupling constant α_s^0 and the pion decay constant F. The spinor ψ describes the proton and neutron fields, while the pion fields are described by the matrix-valued function U, which can be written as [3]:

$$
\begin{aligned}
U &= u^2 = \sigma + i\frac{\phi}{F},\ \ \sigma^2 + \frac{\phi^2}{F^2} = 1, && (8)\\
\phi &= \begin{pmatrix} \pi^0 & \sqrt{2}\pi^- \\ \sqrt{2}\pi^+ & -\pi^0 \end{pmatrix},\ \ Q = \begin{pmatrix} 1 & 0 \\ 0 & 0 \end{pmatrix}\\
\bigtriangledown_\mu U &= \partial_\mu U - ieA_\mu[Q, U] && (9)\\
D_\mu\psi &= \partial_\mu\psi + \Gamma_\mu\psi, && (10)\\
\Gamma_\mu &= \frac{1}{2}\left\{u^\dagger(\partial_\mu - ieA_\mu Q)u + u(\partial_\mu - ieA_\mu Q)u^\dagger\right\} && (11)\\
u_\mu &= iu^\dagger \bigtriangledown_\mu U u^\dagger,\ \ \chi_\pm = u^\dagger\chi u^\dagger \pm u\chi^\dagger u,
\end{aligned}
$$

where the four-vector A^μ represents the photon field. The expression (6) represents the efective Lagrangian for the electromproduction of any pion (π^+, π^-, π^0) off any nucleon (p, n). Let us now restrict the discussion to the production of π^0 off a proton. In this case U in (8) becomes diagonal and consequently $[Q, U] = 0$. This means that the photon can not interact directly with the π^0 because the interaction term in equation (9) is always zero. However, the photon can interact with the proton through (11) in expression (10). The interaction of a proton and a π^0 is described by the second term in (7). We can use these findings and visualize the leading Feynnman graph for the reaction $p(e, e'p)\pi^0$. As shown in figure 2, the proton first absrobs a virtual photon emitted by the scattered electron and after a while the proton gives away this excessive energy in a form of a neutral pion.

Our first order Lagrangian does not include low energy constants that were introduced in equations (4) and (5) of the previous chapter. They appear only in higher order terms [8].

Since the formalism described above is based on very general symmetry properties of QCD, the amplitudes derived from this Lagrangian are expected to describe all processes involving photons nucleons and pions at low energies very accurately. Now that we have determined the ChPT Lagrangian for π^0 electroproduction we have to derive the cross-section [2] from it and try to compare the theory to measurements.

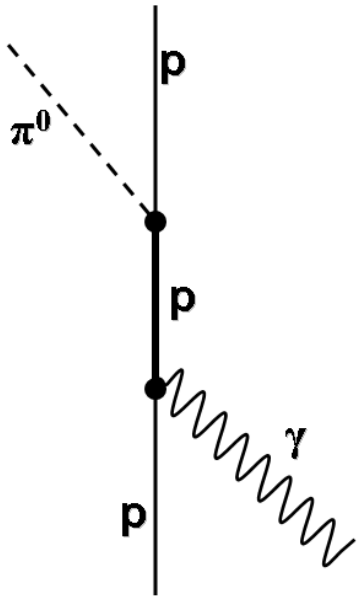

Figure 2: The leading Feynnman graph for the production of the π^0. Virtial photon gives energy to the proton which after a while emits a neutral pion.

3 The Measurements and their problems

3.1 Kinematics

In pion electroproduction experiments the electrons are scattered off the protons in the Hydrogen target (see figure 3). In the one-photon exhange approximation the electron interacts with the protons with a well-defined energy and momentum transfer. The four-momentum vector of the exchanged photon is fixed by the four-momenta of the incident and outgoing electrons:

$$k_i \;=\; \left(\epsilon_i, \vec{k}_i\right), \quad k_f = \left(\epsilon_f, \vec{k}_f\right) \;,\; q = (\omega, \vec{q}) = k_i - k_f \,.$$

The kinematics of a nucleon target (proton) in the initial state is described by $P_i = (E_i, \vec{P}_i)$. After the reaction the recoiled proton has a momentum $P_f = (E_f, \vec{P}_f)$ and emitted pion carries the momentum $k = (\omega_\pi, \vec{k})$. Due to momentum conservation there are three independent momenta at the hadronic vertex (q, P_i, k). Because all reaction products are on-shell ($P_f^2 = m_f^2$ and $k^2 = m_\pi^2$) there are three independent scalars that can be set to various values. We have chosen the following Mandelstain scalars [9]:

$$Q^2, \quad s = W^2 = (P_i + q)^2, \quad u = (P_i - k)^2 \,.$$

The threshold laboratory energy ω_L for the production of a neutral pion π^0 with mass $m_\pi = 134.98\,\mathrm{MeV}$ is obtained by evaluating the variable s in the laboratory and in the centre-of-mass (CMS) frame [9]:

$$\omega_L^{Threshold}\left(Q^2\right) = \frac{(m_f + m_\pi)^2 - m_i^2 + Q^2}{2m_i} \,.$$

For the reaction at $Q^2 = 0$ this gives us:

$$\omega_L^{Threshold}(0) = \frac{(938.27 + 134.98)^2 - 938.27 + 0}{2938.27}\,\mathrm{MeV} = 144.69\,\mathrm{MeV} \,.$$

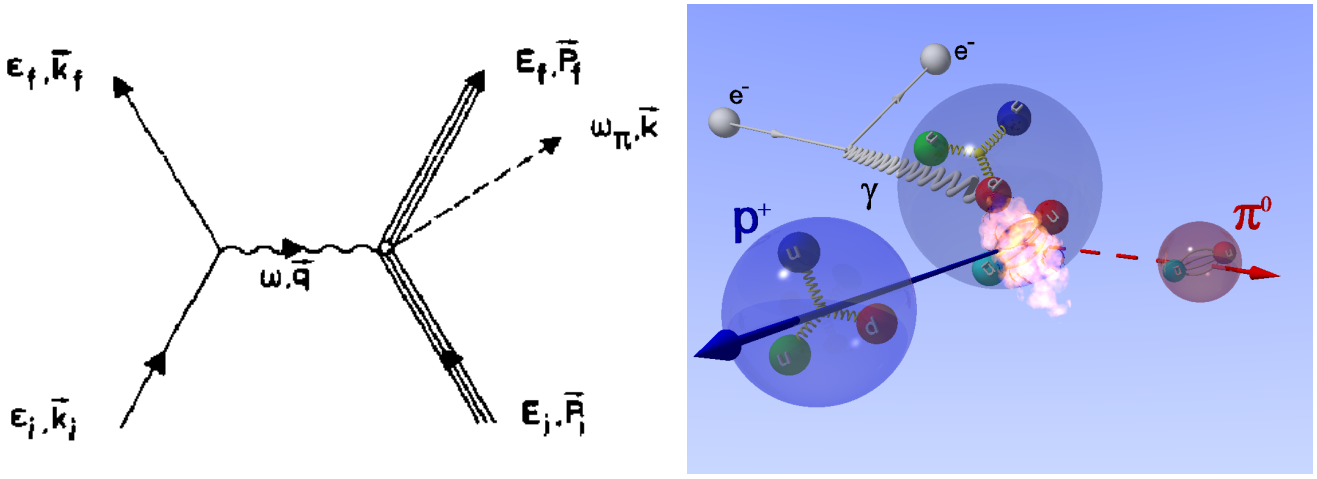

Figure 3: The kinematics variables for a electroproduction experiment in the one-photon exchange approximation.

3.2 Cross-section

The differential cross-section for an exclusive process of a pion electroproduction can be witten as [9]:

$$d\sigma = \frac{\epsilon_i}{k_i}\frac{m_e^2}{\epsilon_i\epsilon_f}\frac{M_i M_f}{E_i E_f}\frac{1}{2\omega_\pi}\frac{d^3k_f}{(2\pi)^3}\frac{d^3k}{(2\pi)^3}\frac{d^3P_f}{(2\pi)^3}(2\pi)^4\delta^{(4)}(P_i+q-k-P_f)\left|\langle P_f,k|J^\mu|P_i\rangle\frac{1}{q^2}\langle k_f|j_\mu|k_i\rangle\right|^2, \quad (12)$$

where all kinematical variables are defined in figure 3. In this cross-section we have considered only the $\frac{1}{q^2}$ electromagnetic interaction, where j_μ is the electron current and J_μ the current of the hadronic system. The current of the electron can be exactly written in terms of Dirac spinors $u(k)$ and Dirac matrices γ^μ as [5]:

$$j^\mu = -e\overline{u}(k')\gamma^\mu u(k)e^{i(k'-k)\cdot x}$$

On the other hand the current of the hadronic system has a more complex form. This is due to the fact that the proton has an extended structure and that in the final state we get two hadrons: the pion and the proton. Therefore we write a most general form of a transition current between the initial and final nucleon states which reflects the negative parity of the pion [9]:

$$\begin{aligned} J^\mu = \overline{\psi}(p')\Bigg\{&\left[A\left(\gamma_\mu - (\gamma\cdot\frac{q}{q^2})q_\mu\right) + B\frac{1}{2}(P_i+P_f) + Ck_\mu\right]\gamma_5 \\ &+ \left[D\left(\gamma_\mu - (\gamma\cdot\frac{q}{q^2})q_\mu\right) + E\frac{1}{2}(P_i+P_f) + Fk_\mu\right]\gamma_5\not{q}\Bigg\}\psi(p) \end{aligned} \quad (13)$$

We define two independent unit vectors $\hat{k} = \frac{\vec{k}}{k}$ and $\hat{q} = \frac{\vec{q}}{q}$, that specify the reaction plane (see figure 4) in the center-of-mass system.

When the usual forms of the Dirac matrices and spinors are inserted, the current operator $\hat{J}^\mu$

can be rewritten in the following form [9]:

$$\begin{aligned}
\hat{J}^{\mu} &= (\hat{\rho}, \hat{\vec{J}}) \\
\hat{\vec{J}} &= \frac{4\pi W}{m}\Big[i\left(\vec{\sigma} - (\vec{\sigma}\cdot\hat{q})\hat{q}\right)F_1 + (\vec{\sigma}\cdot\hat{k})(\sigma\times\hat{q})F_2 + i\hat{k}(\vec{\sigma}\cdot\hat{q})F_3 \\
&\quad + i\hat{k}(\vec{\sigma}\cdot\hat{k})F_4 + i\hat{q}(\vec{\sigma}\cdot\hat{q})F_5 + i\hat{q}(\vec{\sigma}\cdot\hat{k})F_6\Big] \qquad (14) \\
\hat{\rho} &= \frac{\vec{q}\cdot\hat{\vec{J}}}{\omega}
\end{aligned}$$

In (14) six so-called structure functions $F_1, F_2, F_3, F_4, F_5, F_6$ appear instead of parameters A, B, C, D, E and F in (13). These structure functions are the generalizations of form-factors in the Rosenbluth formula [5] for elastic electon scattering of a proton but for the more complex process of pion electroproduction. From a more detailed analysis of a structure of each term in (14) it follows [10] that the F_1, F_2, F_3 and F_4 describe the transverse current while the longitudinal component is given by F_5 and F_6.

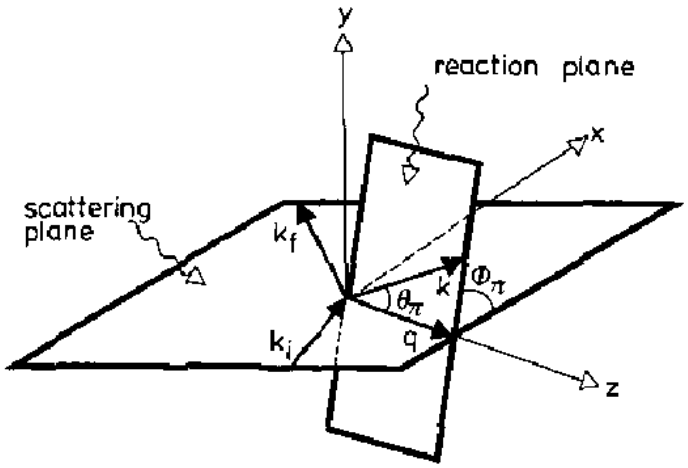

Figure 4: The kinematics for a typical coincidence experiment, leading to an out-of-plane production of a pion [9].

The structure functions depend on three parameters kinematical quantities Q^2, θ_{CM}, W and can be expanded in terms of the Legendre polynomials P_l:

$$\begin{aligned}
F_1 &= \sum_{i\geq 0}\left\{(lM_{l+} + E_{l+})P'_{l+1} + \left[(l+1)M_{l-} + E_{l-}\right]P'_{l-1}\right\} \\
F_2 &= \sum_{l\geq 1}\left[(l+1)M_{l+} + lM_{l-}\right]P'_l \\
F_3 &= \sum_{l\geq 1}\left[\left(E_{l+} - M_{l+}\right)P''_{l+1} + \left(E_{l-} + M_{l-}\right)P''_{l-1}\right] \\
F_4 &= \sum_{l\geq 2}\left(M_{l+} - E_{l+} - M_{l-} - E_{l-}\right)P''_l \qquad (15) \\
F_5 &= \sum_{l\geq 0}\left[(l+1)L_{l+}P'_{l+1} - lL_{l-}P'_{l-1}\right] \\
F_6 &= \sum_{l\geq 1}\left[lL_{l-} - (l+1)L_{l+}\right]P'_l
\end{aligned}$$

The Legendre polynomials depend on the polar angle of the pion θ_π^{CM}. The physics of the process is captured in the coefficients of this polynomial expansion, the so-called pion production multipoles $M_{l\pm}$ (magnetic multipole), $E_{l\pm}$ (electric multipole) and $L_{l\pm}$ (longitudinal mulitpole). Each multipole tells us about the interaction of a particular angular momentum component of a virtual photon with the hadron system. Multipoles are functions of both energy W and momentum transfer Q^2. The multipoles with $l = 0$ are called s-wave multipoles, those with $l = 1$ are called p-wave multipoles, etc. The way these multipoles depend on Q^2 and W is to be determined by the experiment. The threshold behaviour of all multipoles can be derived from elementary analyticity properties [10], and have the following dependence on the $|q = \vec{q}|$ and $|k = \vec{k}|$:

$$\begin{aligned} E_{l+} &\sim q^l k^l, \;\; L_{l+} \sim q^l k^l, \;\; l \geq 0, \\ M_{l+} &\sim q^l k^l, \;\; M_{l-} \sim q^l k^l, \;\; l \geq 1, \\ E_{l-} &\sim q^{l-2} k^l, \;\; L_{l-} \sim q^{l-2} k^l, \;\; l \geq 2, \end{aligned} \tag{16}$$

The unpolarized coincidence cross-section for the pion electroproduction in the one photon exchange approximation has the form [9, 11]:

$$\begin{aligned} \frac{d\sigma}{d\Omega_f d\epsilon_f d\Omega_\pi} &= \Gamma \left(\frac{d\sigma_T}{d\Omega_\pi} + \epsilon_L \frac{d\sigma_L}{d\Omega_\pi} + [2\epsilon_L(1+\epsilon)]^{\frac{1}{2}} \frac{d\sigma_{TL}}{d\Omega_\pi} \cos\phi_\pi + \epsilon \frac{d\sigma_{TT}}{d\Omega_\pi} \cos 1\phi_\pi \right), \\ \epsilon &= \frac{1}{1 + 2\frac{\vec{q}^2}{Q^2} \tan^2 \frac{1}{2}\theta_e}, \;\; \epsilon_L = \epsilon \frac{Q^2}{\omega^2}, \\ \Gamma &= \frac{\alpha}{2\pi^2} \frac{\epsilon_f}{\epsilon_i} \frac{(W^2 - m_i^2)}{2 m_i Q^2} \frac{1}{1-\epsilon} \end{aligned} \tag{17}$$

where Γ represents the virtual photon flux, ω^* is the photon energy and ϵ the transverse polarization. θ_π and ϕ_π are angles relative to the momentum transfer $\vec{q}$ given in the CMS-frame, and $\vec{q}$ and θ_e must be evaluated in the laboratory frame. The first two terms in the (17) are refered to as the transverse (T) and longitudinal (L) cross-section and they do not depend on the azimutal angle ϕ_π. The third and fourth term describe the tansverse-longitudinal interference (TL) and a transverse-transverse interference (TT) which both depend on angle ϕ_π. All cross-sections ($\frac{d\sigma_i}{d\Omega}$) can be expressed in terms of structure functions (15). The longitudinal and transversal term, for example, can be after integration expressed as:

$$\begin{aligned} \sigma_T &= \int \frac{d\sigma_T}{d\Omega_\pi} d\Omega_\pi = \\ &= 2\pi \frac{|\vec{k}|}{k_\gamma^{CM}} \sum_{l=0}^{\infty} (l+1)^2 \left[(l+2) \left(|E_{l+}|^2 + |M_{(l+1)-}|^2 \right) + l \left(|M_{l+}|^2 + |E_{(l+1)-}|^2 \right) \right] \\ \sigma_L &= \int \frac{d\sigma_L}{d\Omega_\pi} d\Omega_\pi = 2\pi \frac{|\vec{k}|}{k_\gamma^{CM}} \sum_{l=0}^{\infty} (l+1)^3 \left(|L_{l+}|^2 + |L_{l-}|^2 \right) \end{aligned}$$

3.3 Current Results and their problems

There has been a considerable effort in the investigation of the electroproduction of neutral pions near the threshold [12]. Measurements of the lowest contributing multipole (E_{0+}) were made at Mainz. From figure 5 we see, that they agree well with the ChPT. These measurements are possible because near the threshold neutral pion production cross-section is dominated by the

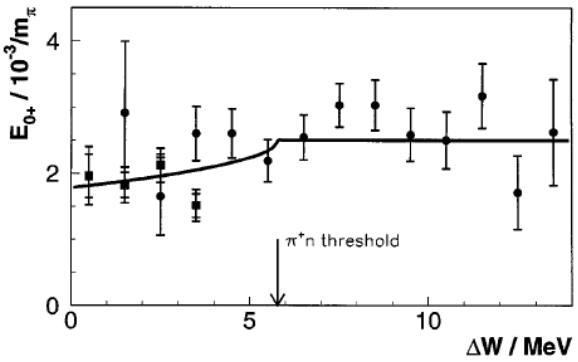

Figure 5: The results for the real part of the amplitude E_{0+} around the threshold for the pion electroproduction. Data points represented with squares are from Mainz, and with circles from NIKHEF [13].

s-wave amplitudes E_{0+} and L_{0+}. From (16) can be seen, that at the threshold these multipoles are all that survives. All other multipoles are zero. On the other hand, high precision measurements of electroproduction at $Q^2 = 0.10\,[\mathrm{GeV}]^2$ [13] and $0.05\,[\mathrm{GeV}]^2$ [11] tell a different story. ChPT calculations were fit to the $Q^2 = 0.10\,[\mathrm{GeV}]^2$ data to determine the low energy constants. When they have compared these results to the ChPT predictions of the $0.05\,[\mathrm{GeV}]^2$ data, they discovered a big difference between these two. Discrepencies were observed both at threshold and at higher values of W [12].

Figure 6 shows the existing high-precision measurements of the total cross-section for the π^0 production as a function of ΔW and Q^2. The solid line in these graphs represents the ChPT calculations. We can clearly see a striking difference between the calculation and the precise data from Mainz. Figure 7 shows how the L_{0+} amplitude depends on the ΔW. Again we can see that the ChPT calculation does not provide a good representation of the data. Discrep-

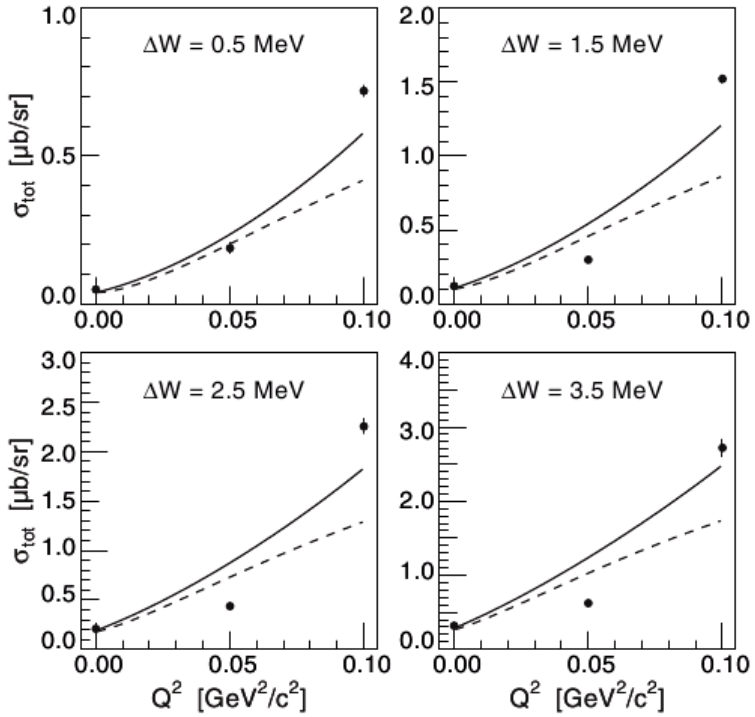

Figure 6: The total cross-section σ_{tot} versus Q^2, at a value of $\epsilon = 0.8$. The solid line is the prediction of ChPT. [11].

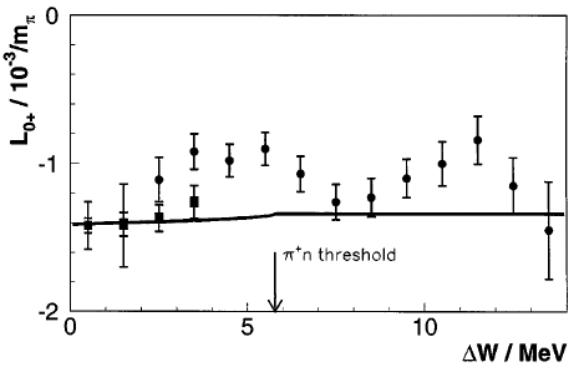

Figure 7: The results for the real part of the amplitude L_{0+} around the threshold for the pion electroproduction. Data points represented with squares are from Mainz [13], and with circles from NIKHEF.

ancies are also observed between the measured differential longitudinal-transverse cross-section at $Q^2 = 0.05\,[\mathrm{GeV}]^2$ for different energies ΔW above the threshold and the predictions of the ChPT (see figure 8). It is evident that the differences get worse as ΔW increases. There appear

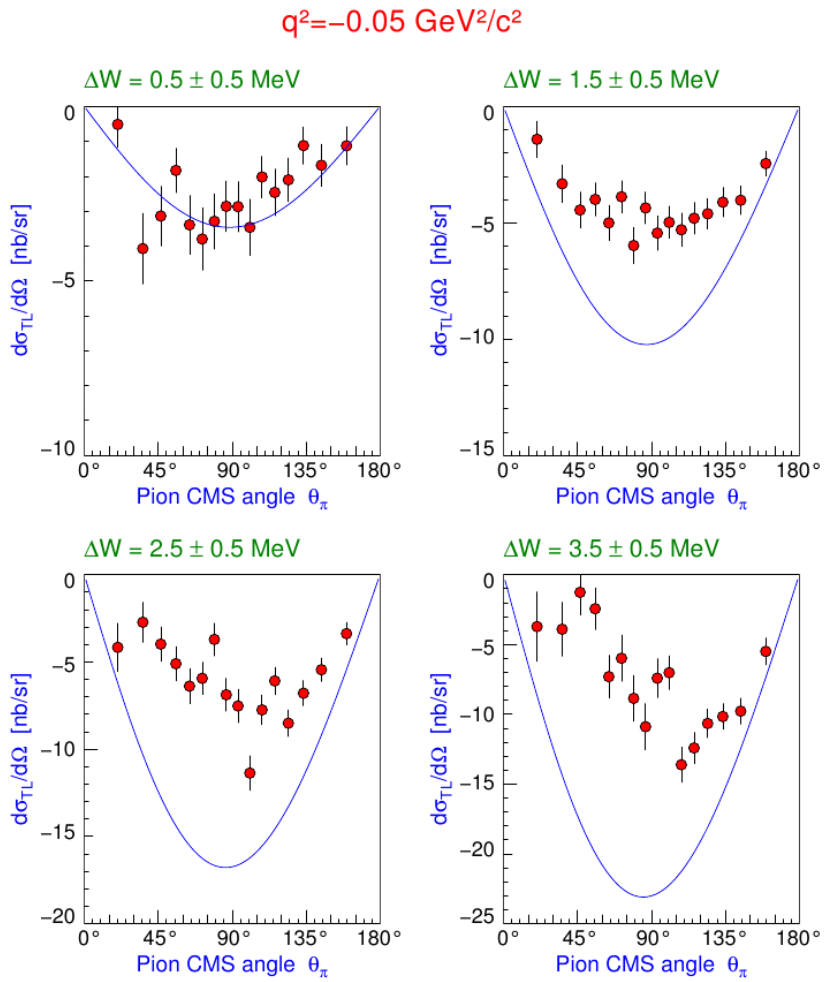

Figure 8: Differential longitudinal-transverse cross-section for $Q^2 = 0.05\,[\mathrm{GeV}]^2$ and different ΔW determined by e-vertex. The solid lines represent the results of ChPT, for which low energy constants were derived from measurements at $Q^2 = 0.10\,[\mathrm{GeV}]^2$. Large discrepancies which increase with ΔW are observed [12].

to be many differences between the measured data and the predictions of the chiral perturbation theory, which at present, are unresolved. If these issues remain unsolved, they will constitute a serious threat to the viability of the ChPT as a useful theory of dynamical processes. Such a result would be very problematical as ChPT is firmly grounded in the basic properties of the QCD.

There are several possible options which could resolve these discrepancies. Maybe it is necessary to include a significantly larger number of terms in the Chiral expansion, thereby increasing the number of low energy constants to be determined empirically from the $Q^2 = 0.10\,[\mathrm{GeV}]^2$ data. If new, precise data at $0.05\,[\mathrm{GeV}]^2$ would be used to determine the low energy constants and the resulting calculation would reproduce the evaluation of the data in region around $0.05\,[\mathrm{GeV}]^2$ but would fail when approaching to $0.10\,[\mathrm{GeV}]^2$, than this would be a favored explanation. Another possibility is that one or more data points are incorrect. This question can only ne answered by obtaining new, high statistics data. In the region near the threshold only S-wave and P-wave multipole amplitudes are significant. The contibution of S-waves is approximately constant near the threshold, while the contribution of the P-wavs increases with the energy above threshold. Since we know from figure 8 that dicrepancy between ChPT and measured data rises with the Q^2 this would suggest a serious problem with P-waves. To obtain a better understanding of the S- and P-wave contributions to the cross-section, it is again necessary to gather more precise data in the threshold region. It is also possible that there is something basically wrong with the formulation of the Chiral perturbation theory. If experimental results can be reconciled and still can not be reproduced by the theory, than this would also be a possible explanation.

4 New Threshold π^0 Experiment at JLab

In order to resolve the discrepancies and questions decribed in section 3.3 the scientists at the Thomas Jefferson National Accelerator Facility have decided to perform a high precision measurement of the reaction $p(e, e'p)\pi^0$ near threshold [12] on a fine grid of Q^2 and ΔW. With these measurements they will be able to to extend and re-examine existing measurements of electroproduction near threshold, in particular those from Mainz [13, 11] and provide a strong test of chiral QCD dynamics. The experiment was performed by the Hall A Collaboration using a high-resolution spectrometers (HRS) in coincidence with the BigBite spectrometer.

4.1 Hall-A Collaboration

The Continuous Electron Beam Accelerator Facility (CEBAF) at Jefferson Lab (see figure 9) was built to investigate the structure of nuclei and hadrons in the region below the high-energy regime at intermediate energies and the underlying fundamental interactions. CEBAF's 6 GeV, polarized continuous wave electron beam is an ideal probe for the study of non-perturbative QCD. The beam is delivered independently to JLab's three experimental Halls A, B and C. All Halls can simultaneously receive the maximum energy beam.

The instrumentation in Hall A [14] was designed to study electro- and photo-induced reactions at very high luminosity and good momentum and angular resolution. The research program is aimed at a variety of subjects, including nucleon form factors, nucleon electromagnetic and spin structure fuctions, and properties of the nuclear medium. The central components of Hall A are two high-resolution spectrometers HRS-L and HRS-R (see figure 10). They consist of three quadrupole and a dipole superconducting magnets in the QQDQ magnet configuration. With carefull planning and engineering they have achieved a high momentum resolution at 1×10^{-4} level over the 0.8 to 4.0 GeV/c momentum range, a large acceptance in both angle and momentum, good position and angular resolution in the scattering plane, an extended target acceptance and a large angular range. For the exact characteristics of spectrometers see table 1. Beside the HRS spectrometers there is also a BigBite spectrometer [15]. The spectrometer consists of a single normal-conducting dipole magnet and combines a large solid angle with a large momentum

a.)  b.) 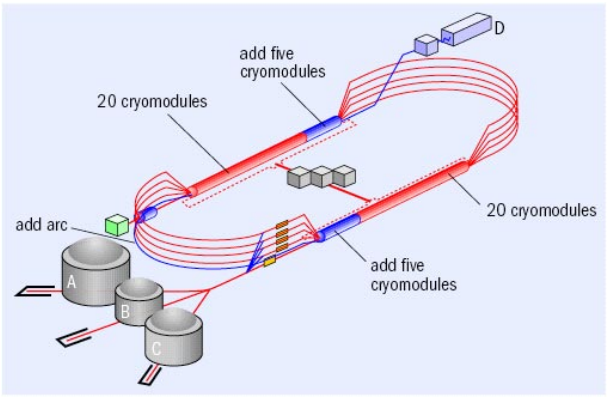

Figure 9: a.) An image of the TJNAF center. The three small hills conceal the three underground experimental halls. b.) The schematic view of the CEBAF accelerator complex. The electron beam from the accelerator is delivered to three experimental halls A, B and C.

a.) 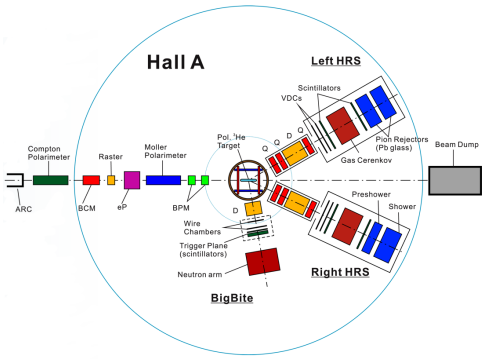

b.) 

c.)  d.) 

Figure 10: a.)Spectrometer layout in Hall-A. There are three spectrometers: Two high resolution spectrometers HRS-L, HRS-R and a large-acceptance spectrometer BigBite. All three spectrometers can be positioned at various scattering angles. b.) The BigBite spectrometer during the $p(e, e'p)\pi^0$ experiment. c.) and d.) The HRS-L spectrometer. The optical length of this spectrometer is 23.4 m.

acceptance (see table 1).

Main design characteristics of HRS's [14]	
Configuration	QQDQ
Momentum range	$0.3 - 4.0$ GeV/c
Momentum acceptance	$-4.5\% \leq \frac{\delta p}{p} \leq 4.5\%$
Momentum resolution	1×10^{-4}
Angular acceptance	
Horizontal	± 30 mrad
Vertical	± 60 mrad
Angular resolution	
Horizontal	0.5 mrad
Vertical	1.0 mrad

Main design characteristics of BigBite [15]	
Configuration	Dipole
Momentum range	$200 - 900$ MeV/c
Momentum acceptance	$-0.6 \leq \frac{\delta p}{p} \leq 0.8$
Momentum resolution	4×10^{-3}
Angular acceptance	≈ 100 msr
Angular resolution	≈ 1 msr

Table 1: Main design characteristics of the Hall-A high resolution spectrometers HRS and new BigBite spectrometer.

4.2 The experimental setup

The intent of the Threshold Pi0 experiment (E04-007) has been to study the$p(e, e'p)\pi^0$ reaction in the range of $0.04\,[\mathrm{GeV}]^2 \leq Q^2 \leq 0.14\,[\mathrm{GeV}]^2$ and $0\,\mathrm{MeV} \leq \Delta W \leq 20\,\mathrm{MeV}$. We have used BigBite spectrometer to detect the protons and the HRS-L to detect the electrons. The high resolution of the electron spectrometer allowed a precise determination of the invariant mass W and the three momentum transfer $\vec{q}$. On the other hand, the large acceptance and momentum range of BigBite permitted a large fraction of the cone of forward-emitted protons along $\vec{q}$ to be detected simultaneously. As a target we have used a 10 cm-long and 2 cm-wide liquid hydrogen cell with thin Havar windows and walls. The HRS-R spectrometer was used as a single-arm electron detector to monitor the luminosity throughout the experiment.

4.3 Current Results

The experiment E04-007 was running in April and May 2008. Since then the data analysis is underway. The data analysis is at the moment focused on the calibration of the BigBite spectrometer. In this experiment a new set of detectors has been used for this spectrometer and because of these modifications its optic properties have changed. Figure 11 shows the missing mass peak (which should be centered at the pion mass) after first and second iterations of the calibration. We expect to have the first preliminary results on the measured cross-sections analysis by early 2009.

5 Conclusion

Nuclear reactions in the low-energy limit are very hard to describe. Strong interactions between quarks inside hadrons can not be approximated with one- or two-gluon exchange like at high energies. Many gluons are exchanged in each reaction and that makes these processes impossible to describe in terms of perturbative QCD. Suitable phenomenological models are needed to describe the reactions at low energies. These approaches are firmly grounded in the symmetries of QCD. Any dissagrement between the theory and the measurements would pose a fundamental problem. Current measurements are showing such dissagrements but they are very inconclusive. There are many possible explanations why the theory and the measured data are inconsistent. Therefore it is of great importance to make new and more precise measurements near the threshold, like

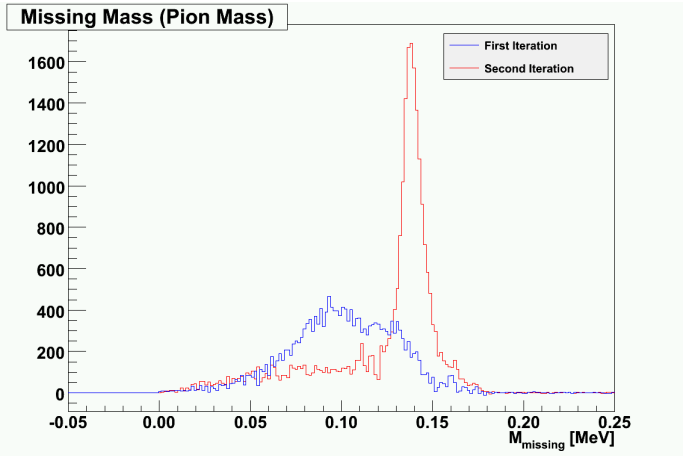

Figure 11: Graph shows the missing mass peak in the Threshold Pi0 experiment which corresponds to the mass of the pion: $M^2_{miss} = (\omega - T_p)^2 - (\vec{q} - \vec{p_p})^2$, where T_p is the kinetic energy of the proton and p_p is its momentum.

these in JLab, and try to resolve the discrepency between the two. Hopefuly we will learn the true answer in the next few years.

References

[1] Wikipedia, *Quantum chromodynamics*, `http://en.wikipedia.org/wiki/Quantum_chromodynamics`, (1.12.2008)

[2] M. E. Peskin D. V. Schroeder, An Introduction to *Quantum Field Theory*, Westview Press, 1995

[3] V. Bernard *et al.*, *Chiral perturbation theory*, arXiv:hep-ph/0611231v1, 17 Nov 2006

[4] C. Amsler et al., *Phys. Lett.* **B667**, 1 (2008)

[5] F. Halzen A. D. Martin, *Quarks and Leptons*, An Introductory Course in Modern particle Physics, John Wiley & Sons. Inc.

[6] Wikipedia, *Chiral perturbation theory*, `http://en.wikipedia.org/wiki/Chiral_perturbation_theory`, (15.12.2008)

[7] J. F. Donoghue *et al.*, *Dynamics of the Standard Model*, Cambridge University Press, 1992

[8] V. Bernard *et al.*, *Physics Reports*, **246**, 315-363, 1994

[9] D. Drechsel *et al.*, *J. Phys. G: Nucl. Part. Phys.* **18**, 449(1992)

[10] E. Amaldi *et al.*, *Pion-Electroproduction*, Springer-Verlag, Berlin 1979

[11] H. Merkel *et al.*, *Phys. Rev. Lett.* **88**, 012301 (2001)

[12] R. Lindgren *et al.*, *E04-007 Threshold π^0 Production*, Jefferson Lab PAC25 Proposal, December 2003

[13] M.O. Distler *et al.*, *Phys. Rev. Lett.* **80**, 2294 (1998)

[14] J. Alcorn *et al.*, Nucl. Instr. and Meth. **A 522** (2004) 294

[15] D.J.J. Lange *et al.*, Nucl. Instr. and Meth. **A 406** (1998) 182